

Shaken, not stirred: Test particles in binary black hole mergers

Pieter vd Merwe^{a,*} and Markus Böttcher^a

^aCentre for Space Research, North-West University,
Potchefstroom, 2520, South Africa

E-mail: pietervdmerwejnr@gmail.com, Markus.Bottcher@nwu.ac.za

Since 2015 the advanced Laser Interferometer Gravitational-Wave Observatory (aLIGO) has detected a large number of gravitational wave events, originating from both binary neutron stars and binary black hole (BBH) mergers. In light of these detections, we simulate the dynamics of ambient test particles in the gravitational potential well of a BBH system close to its inspiral phase with the goal of simulating the associated electromagnetic radiation and resulting spectral energy distribution of such a BBH system. This could shed light on possible detection ranges of electromagnetic counterparts to BBH mergers. The potentials are numerically calculated using finite difference methods, under the assumption of non-rotating black holes with the post-Newtonian Paczynski-Wiita potential approximation in tandem with retarded time concepts analogous to electrodynamics. We find that the frequencies of potential electromagnetic radiation produced by these systems (possibly reaching Earth), range between a few kHz to a few 100MHz.

High Energy Astrophysics in Southern Africa 2022 - HEASA2022
28 September - 1 October 2022
Brandfort, South Africa

*Speaker

1. Introduction

Since the detection of the first gravitational wave (GW) event in 2015 by aLIGO [1, 2], multiple binary black hole (BBH), binary neutron star (BNS), and black hole - neutron star mergers have been detected [3–8], with many new prospects for future detectors such as the laser interferometer space antenna (LISA) [9, 10] and the Einstein telescope [11, 12]. With these detections, a new window on multi-messenger astronomy has opened and the search for multiple messengers (gravitational waves, particles, and photons) from various sources began [13–21].

Coincident with the detection of the first GW event, the *Fermi* gamma-ray burst monitor (GBM) detected a weak transient gamma-ray burst (GRB) signal (GW150914-GBM) of 1s duration, 0.4s after the BBH merger event GW150914, with a consistent sky localization [22, 23]. The GRB was found during an off-line analysis of the Fermi GBM data [24, 25]. This possible electromagnetic (EM) counterpart to a BBH merger event is highly unexpected and, as such, led to many speculations and counter arguments regarding possible scenarios that could produce observable EM signals from a BBH merger [26–32], and the possible GRB application thereof should the detection be valid [33, 34]. It is believed that GW events resulting from stellar-mass BBH mergers are unlikely to have EM counterparts [35]. However, the detection of GW150914-GBM encouraged theoretical speculation on possible scenarios in which EM counterparts to GW signals are possible.

In light of these findings, we develop a naïve, pseudo-Newtonian exploratory code using the Paczynski-Wiita potential and retarded time concept to investigate accelerations and possible spectral energy distribution (SED) forms obtainable from evolving ambient particles present in a BBH merger system (in the inspiral phase) under the influence of gravity. Since this is intended as a naïve exploratory code to possibly be further built upon later, the addition of accretion disk considerations and fully general relativistic magnetohydrodynamic simulations such as those done by [36] have been neglected in this work. In section 2, we give a brief overview of the building blocks used to develop the model and the code. Section 3 shows a set of test results obtained from the code. A discussion on the test results and future prospects is given in section 4.

2. The model

This section describes the model used to determine the gravitational acceleration of a charged particle in an inspiral-phase BBH system. The gravitational acceleration of the particle is determined using the Paczynski-Wiita gravitational potential, as described in Section 2.1. Additionally, we introduce the concept of retarded time (analogous to electrodynamics) in order to determine the acceleration of the particle.

The effective one-body (EOB) problem entails treating two bodies, with masses M_1 and M_2 , with a separation $\vec{r} = \vec{r}_2 - \vec{r}_1$, orbiting a common center of mass as a single body with a reduced mass $\mu = \frac{M_1 M_2}{M_1 + M_2}$ under the influence of an external potential due to a total mass $M = M_1 + M_2$. To first post-Newtonian order, the analytical solution of the circularized, inspiral BBH orbit can be derived

$$\text{as } R(t) = R_0 \left(\frac{t_c - t}{t_c} \right)^{-0.25} \frac{M_c}{M}, \quad (1) \quad \text{and,} \quad \Phi(t) = -2 (5M_c)^{-0.625} (t_c - t)^{-0.25}, \quad (2)$$

with t_c the time to coalescence of the BHs, R_0 the initial separation of the BHs, $M_c \equiv \frac{(M_1 M_2)^{0.6}}{(M_1 + M_2)^{0.2}}$ the chirp mass of the BBHs, $R(t)$ the separation as a function of time and $\Phi(t)$ the dimensionless

phase of μ in the center of momentum frame [37]. From this the position vectors \vec{r}_{M_1} and \vec{r}_{M_2} can be found similarly to the classical EOB problem.

2.1 The Paczynski-Wiita Potential

The Paczynski-Wiita potential is an important pseudo-Newtonian approximation to the general relativistic Schwarzschild geometry developed by B. Paczynski and P. Wiita while studying thick accretion disks and super-Eddington luminosities [38]:

$$\Phi_{PW}(r) = -\frac{GM}{r-r_s}, \quad r_s = \frac{2GM}{c^2}. \quad (3)$$

The Paczynski-Wiita potential is a Newton-like potential that (for the case of non-rotating BHs) exactly reproduces the marginally bound ($r_{mb} = 2r_s$) and marginally stable circular ($r_{ms} = 3r_s$) orbits of the Schwarzschild geometry, as well as the form of the Keplerian angular momentum, but not that of the Keplerian angular velocity [39, 40]. [41] has shown that orbits resulting from a Paczynski-Wiita potential exhibit satisfactory correspondence with the exact General relativistic (GR) case, with the caveat that these orbits are likely to be more chaotic than those expected from a fully relativistic approach. Hence, any predictions made in this article regarding particle acceleration and electromagnetic radiation may be considered as upper limits to the radiative output in full GR.

2.2 Calculating the acceleration of a charged particle in an inspiral phase BBH merger

Considering a charged particle, with mass m_e , position \vec{r} , and velocity \vec{v} in the lab frame, if the particle is under the influence of a force $\vec{F} = \frac{d\vec{p}}{dt}$, then to determine \vec{F} , the retarded positions of the BHs, with respect to the position of the charged particle, have to be determined first. For this purpose, we define retarded time $t_r \equiv t - \frac{1}{c} |\vec{r} - \vec{r}_k|$, where \vec{r} is the position of the particle and \vec{r}_k is the position of the BH at time t_r . The retarded times, t_{r,M_1} and t_{r,M_2} , at which to evaluate the position vectors of the two BHs are determined using the Newton-Raphson numerical root-finding method.

Once we have the retarded times t_{r,M_1} and t_{r,M_2} , \vec{F} can be determined. Using the Paczynski-Wiita potential, as described in Section 2.1, where $\Phi_{PW,1}$ and $\Phi_{PW,2}$ denotes the potential resulting from M_1 and M_2 respectfully, we have that

$$\vec{F} = m_e \vec{\nabla} [\Phi_{PW,1}(|\vec{r} - \vec{r}'_1(t_{r,M_1})|) + \Phi_{PW,2}(|\vec{r} - \vec{r}'_2(t_{r,M_2})|)]. \quad (4)$$

Furthermore, it follows that Equation 4 simplifies to

$$\vec{F} = -m_e \left[\frac{GM_1}{r_{d,1}(r_{d,1}-r_{s,1})^2} (x_{d,1}\hat{x} + y_{d,1}\hat{y} + z_{d,1}\hat{z}) + \frac{GM_2}{r_{d,2}(r_{d,2}-r_{s,2})^2} (x_{d,2}\hat{x} + y_{d,2}\hat{y} + z_{d,2}\hat{z}) \right], \quad (5)$$

where $r_{d,k} = |\vec{r} - \vec{r}'_k(t_{r,M_k})|$, $x_{d,k} = (\vec{r} - \vec{r}'_k(t_{r,M_k}))_x$, $y_{d,k} = (\vec{r} - \vec{r}'_k(t_{r,M_k}))_y$, $z_{d,k} = (\vec{r} - \vec{r}'_k(t_{r,M_k}))_z$, and $k = 1, 2$. From the definition $\vec{p} = \gamma m_e \vec{v}$ we have that

$$v^2 = \frac{p^2}{m_e^2} \left(1 + \frac{p^2}{m_e^2 c^2} \right)^{-1}, \quad \text{and} \quad \vec{v} = \frac{\vec{p}}{m_e} \sqrt{1 - \frac{p^2}{m_e^2 c^2} \left(1 + \frac{p^2}{m_e^2 c^2} \right)^{-1}}. \quad (6)$$

For a given velocity we can calculate the position from the definition of velocity, $\vec{v} = \frac{d\vec{r}}{dt}$. Substituting equation 6 into this and converting to geometrized units¹ we find a set of coupled first-order ordinary differential equations (ODEs),

$$\frac{d\vec{p}}{dt} = \vec{F}(t, \vec{r}), \quad \text{and}, \quad \frac{d\vec{r}}{dt} = \frac{\vec{p}}{m_e} \sqrt{1 - \frac{p^2}{m_e^2} \left(1 + \frac{p^2}{m_e^2}\right)^{-1}}, \quad (7)$$

that must be solved simultaneously, with \vec{F} calculated as described in equation 5. In order to simultaneously solve this set of ODEs we use the embedded 7(8) Runge Kutta method devised by [42]. In order to calculate the acceleration \vec{a} of the particle under the influence of the retarded force \vec{F} , the equation

$$\vec{a} = \frac{1}{m\gamma} \left[\vec{F} - (\vec{v} \cdot \vec{F}) \vec{v} \right], \quad (8)$$

is used. Finally, the acceleration of the particle \vec{a} is separated into its parallel, $\vec{a}_{\parallel} = \left(\vec{a} \cdot \frac{\vec{v}}{|\vec{v}|} \right) \hat{v}$, and perpendicular, $\vec{a}_{\perp} = \vec{a} - \vec{a}_{\parallel}$, components, with respect to the motion of the particle.

2.3 Calculating the SED of charged particles in a near-inspiral BBH merger

The SED of a single accelerated charged particle is given by

$$I(\nu) = \frac{\mu_0 q^2}{3\pi c} \left[|\gamma^2(\nu) \vec{a}_{\parallel}(\nu)|^2 + |\gamma^3(\nu) \vec{a}_{\perp}(\nu)|^2 \right]. \quad (9)$$

From this, it is evident that $I_{\parallel,b} = |\gamma^2(\nu_b) \vec{a}_{\parallel}(\nu_b)|^2$, and $I_{\perp,b} = |\gamma^3(\nu_b) \vec{a}_{\perp}(\nu_b)|^2$ needs to be determined in frequency space². This is done by simply taking the discrete Fourier transform of the relevant products:

$$I_{\parallel,b} = \frac{1}{N} \sum_{j=0}^{N-1} \left| \gamma_j^2 \vec{a}_{\parallel,j} \right|^2 e^{-\frac{i2\pi}{N}bj}, \quad (10) \quad I_{\perp,b} = \frac{1}{N} \sum_{j=0}^{N-1} \left| \gamma_j^3 \vec{a}_{\perp,j} \right|^2 e^{-\frac{i2\pi}{N}bj}, \quad (11)$$

with $i = \sqrt{-1}$, $j = 0, 1, \dots, N$ where N is the number of uniformly distributed time domain data points, $b = 0, 1, \dots, N$ [43, 44]. In order to perform the fast Fourier transform (FFT), which requires a set of uniformly spaced data points, the non-uniformly spaced acceleration data is interpolated using cubic spline interpolation.

Equation 9 gives the SED of a single particle. Considering a set of $N_{\text{particles}}$ particles, each with an SED $I_n(\nu)$, the total SED of the system can be found by summing over the SEDs of all of the particles in the system³.

Since it is expected that the radiation contribution of each particle is incoherent, the total SED can be calculated in this manner without the need to consider possible interference when summing over the fluxes of the particles. When considering a set of discrete SEDs $I_n(\nu_b)$ for each particle, however, this process becomes somewhat more complicated. Applying the FFT in the calculation

¹We convert to geometrized units here for better numerical accuracy as terms containing G and c can suffer from numerical rounding errors.

²Here the subscript b only serves to indicate discretization.

³Here $n = 1, \dots, N_{\text{particles}}$

of the SEDs of each of the $N_{particles}$ particles, the implicit discrete frequency steps $d\nu$ within the FFTs are not necessarily of the same size.⁴ To account for this, each individual particle SED $I_n(\nu)$ is interpolated to comparable frequency increments, using cubic spline interpolation.

3. Results

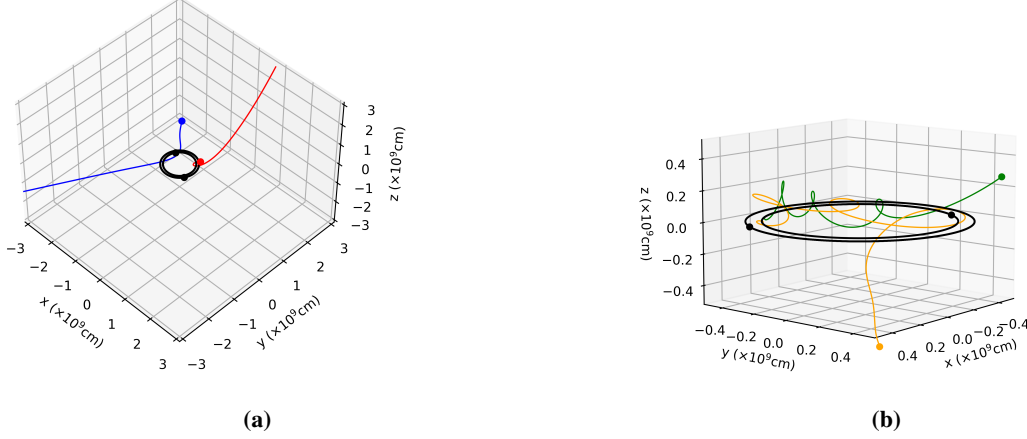


Figure 1: Example of a selection of 4 particles orbiting through an inspiraling BBH system with masses $30M_{\odot}$ and $35M_{\odot}$. Two of the particles are chosen from the subset of particles that escape from the system (panel (a)), with the other two chosen from the subset of the particles that plummet into one of the BHs (panel (b)). The dots indicate the initial position of the particles. The particles used here are taken to be electrons, though the model is independent of the particle mass.

Property	Particle 1	Particle 2	Particle 3	Particle 4
$v_x(\text{cm} \cdot \text{s}^{-1})$	-2.52×10^4	2.33×10^3	3.80×10^3	-6.30×10^4
$v_y(\text{cm} \cdot \text{s}^{-1})$	-1.10×10^3	-1.55×10^3	-1.42×10^3	-4.33×10^3
$v_z(\text{cm} \cdot \text{s}^{-1})$	3.60×10^3	-4.93×10^3	-1.59×10^3	3.02×10^3
$x(\text{cm})$	2.69×10^8	-8.09×10^8	-5.33×10^8	1.47×10^9
$y(\text{cm})$	5.50×10^8	8.96×10^8	4.32×10^8	1.33×10^9
$z(\text{cm})$	-1.42×10^8	6.64×10^8	2.50×10^8	-1.63×10^8

Table 1: Initial conditions of the set of example particles. These values are randomly generated by the code for use in the model.

An example of a selection of the particle orbits produced by the model for BHs of masses $M_1 = 30M_{\odot}$ and $M_2 = 35M_{\odot}$, with an initial separation of 10^9cm , is given in figure 1, with initial positions and velocities summarised in table 1. Of the 1060 particles evolved through the system, 150 show orbits plummeting into one of the BHs. Figure 2 shows the corresponding speed (panel (a)) and acceleration components (panel (b)) of the particles shown in figure 1. As is evident in panel (a) of figure 2, the speeds of the plummeting particles approach the speed of light, while the

⁴This comes from the fact that the size N of the input data set of the FFT will not be the same size for each particle and correspondingly ν_b (the set of discretized frequencies for each particle) will also be at different frequencies for each particle.

particles that leave the system show an initial significant increase in speed, however, this stabilizes as the particles escape the system. Figure 3 shows the individual SEDs of 2 of the selected example particles. The escaping particle SED of particle 1 (panel (a)) shows a drop-off at $\sim 10^1$ Hz and a negligible amplitude. The SED of particle 3 (panel (b)) that plummets into one of the BHs, shows a drop-off at a much higher frequencies ($\sim 10^8$ Hz). Figure 4a shows the total SED of all the particles evolved through the system.

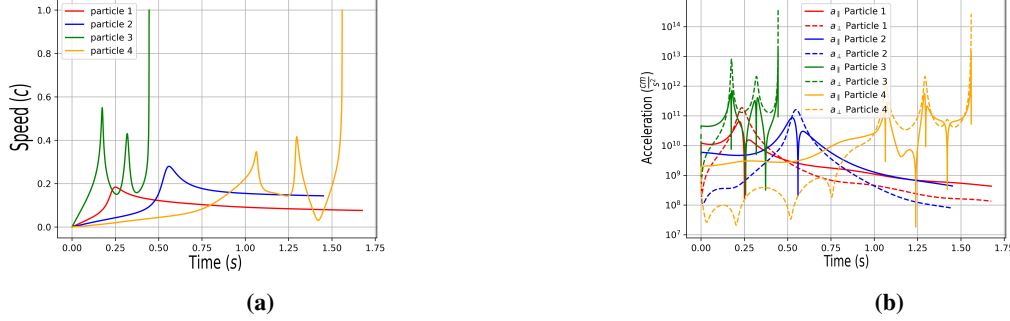


Figure 2: The speed (panel (a)) and acceleration components (panel (b)) of the selection of example particles as they orbit through the BBH inspiral system. In both panels (a) and (b) the peaks correspond to the particles orbiting close to one of the BHs in the system, with the final rise of particles 3 and 4 corresponding with the particles plummeting into one of the BHs.

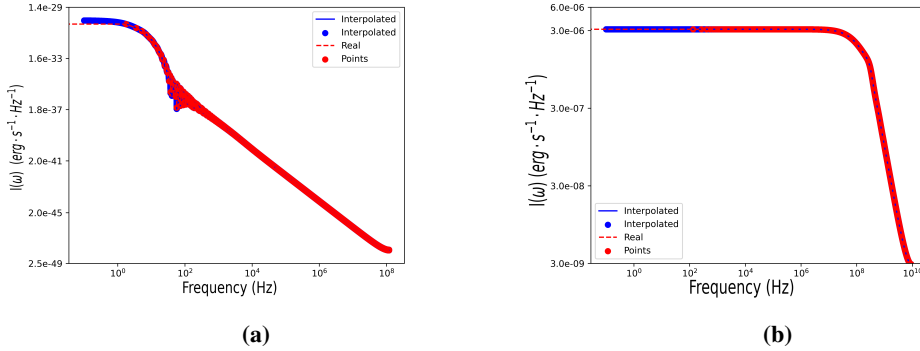
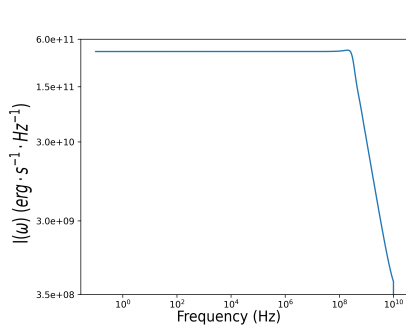


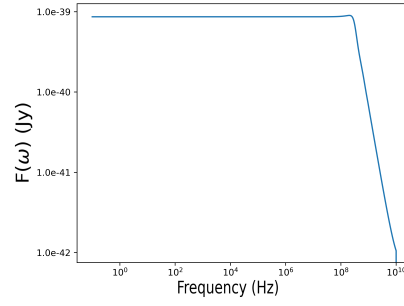
Figure 3: Individual SEDs of the selection of 2 of the example particles. Panel (a) shows the SED of particle 1. This particle shows an orbit that escapes from the system and has a drop-off that occurs at around $\sim 10^1$ Hz. Panel (b) shows the SED of particle 3. This particle has an orbit that plummets into one of the BHs and shows a higher amplitude than that of particle 1. The SED of particle 3 (panel (b)) shows a drop-off at around $\sim 10^8$ Hz.

4. Discussion and Conclusion

The majority of particles are ejected from the system, leading to a significant drop-off in their radiation output at $\sim 10^1$ Hz, an example of which can be seen in figure 3 (panel (a)). A quick order-of-magnitude estimate using the gravitational orbital frequency $\omega_{orb} = \sqrt{\frac{GM}{a^3}} \sim 3$ Hz, with $a \sim 10^9$ cm the characteristic radius of non-plummeting orbits, reveals that this drop-off can likely



(a) Total SED from particles evolved through the inspiraling BBH system, with a steep drop-off occurring at $\sim 10^8$ Hz.



(b) Estimated flux density reaching Earth for an assumed particle density of 10^6 cm^{-3} in a spherical volume of radius $R_V = 10^{10} \text{ cm}$ for the system, with the system assumed to be a distance of $\sim 400 \text{ Mpc}$ from the earth.

Figure 4: The total SED (a) and an estimate of the flux density reaching Earth(b).

be attributed to the orbital frequency of particles orbiting in the system. In contrast to this a handful of the particles plummet into one of the BHs. As can be seen in figure 3 (panel (b)), the SEDs of these particles show a drop-off at significantly higher frequencies ($\sim 10^8 \text{ Hz}$). The higher drop-off frequency for the plummeting particles can likely be attributed to the chaotic orbits of these particles on the scale of the Schwarzschild radii of the black holes. However, another order-of-magnitude estimate taking $a \sim R_{s,k}$, with $k = 1, 2$, shows that $\omega_1 \sim 3.3 \times 10^3 \text{ Hz}$, and $\omega_2 \sim 2.9 \times 10^3 \text{ Hz}$, indicating that the drop-off must be due to chaotic motion on even smaller scales. The total SED of the system shown in figure 4a indicates that the SEDs of the plummeting particles completely dominate the radiative output.

If we consider that the interstellar medium (ISM) plasma frequency is $\sim 2 \text{ kHz}$ (for an assumed electron density of 0.03 cm^{-3}), we know that radiation emitted at frequencies below this threshold will be absorbed by the ISM. As such, only radiation emitted in the range between $\sim 2 \text{ kHz}$ and $\sim 100 \text{ MHz}$ will emerge from the system and be detectable from Earth. Furthermore, from figure 4a, it is also evident that our model predicts that the bulk of possible EM radiation that originates from charged particles accelerated in a BBH merger is distributed at frequencies close to or below the lower end of the sensitivity ranges of current low-frequency radio telescopes. The current sensitivity range of the Low-Frequency Array (LOFAR) is $10 - 240 \text{ MHz}$ [45]. As such, it may be possible to detect radiation due to charged particles accelerated in inspiraling BBH system using LOFAR or other radio telescopes operating in a similar range given a strong enough signal. In order to estimate a rough flux density $F(\omega)$ as a function of frequency for our results, we rescale the total SED in figure 4a for 4.2×10^{36} particles, based on an assumed particle density of 10^6 cm^{-3} in a volume of radius $R_V = 10^{10} \text{ cm}$ for the system⁵. Placing the system at a distance of $\sim 400 \text{ Mpc}$ from the earth, which is consistent with that of GW150914 [1], the estimated flux density $F(\omega)$ can be seen in figure 4b. Comparing the extremely low estimated flux density of the system with the $\mu \text{ Jy}$ sensitivity of LOFAR [46], it is apparent that these events will not be detectable from Earth if only acceleration due to gravity is considered.

⁵The assumed particle density assumed here is just a Highly optimistic guess based on the ISM particle density which is typically several orders of magnitude lower than this.

5. Acknowledgements

This work is based on the research supported in part by the National Research Foundation of South Africa (Grant Number 144799) and in part by the National Astrophysics and Space Science Program of South Africa.

References

- [1] LIGO SCIENTIFIC COLLABORATION AND VIRGO COLLABORATION collaboration, *Observation of gravitational waves from a binary black hole merger*, *Phys. Rev. Lett.* **116** (2016) 061102.
- [2] D. Castelvechi and A. Witze, *Einstein’s gravitational waves found at last*, *Nature news* **11** (2016) .
- [3] LIGO, VIRGO collaboration, *Results from the O3 observing run of the LIGO/VIRGO collaboration*, *PoS HEASA2021* (2022) 060.
- [4] The LIGO Scientific Collaboration, The Virgo Collaboration, The KAGRA Collaboration, R. Abbott, T.D. Abbott, F. Acernese et al., *GWTC-3: Compact binary coalescences observed by LIGO and Virgo during the second part of the third observing run*, *arXiv e-prints* (2021) [arXiv:2111.03606](https://arxiv.org/abs/2111.03606).
- [5] B.P. Abbott, R. Abbott, T.D. Abbott, S. Abraham, F. Acernese, K. Ackley et al., *Binary black hole population properties inferred from the first and second observing runs of advanced LIGO and advanced Virgo*, *The Astrophysical Journal* **882** (2019) L24.
- [6] LIGO SCIENTIFIC COLLABORATION AND VIRGO COLLABORATION collaboration, *Gwtc-1: A gravitational-wave transient catalog of compact binary mergers observed by LIGO and Virgo during the first and second observing runs*, *Phys. Rev. X* **9** (2019) 031040.
- [7] B.P. Abbott, R. Abbott, T.D. Abbott, S. Abraham, F. Acernese, K. Ackley et al., *Low-latency gravitational-wave alerts for multimessenger astronomy during the second advanced LIGO and virgo observing run*, *The Astrophysical Journal* **875** (2019) 161.
- [8] R. Abbott, T.D. Abbott, S. Abraham, F. Acernese, K. Ackley, A. Adams et al., *Observation of gravitational waves from two neutron star–black hole coalescences*, *The Astrophysical Journal Letters* **915** (2021) L5.
- [9] S.L. Larson, *Lisa: A modern astrophysical observatory*, *Proc. of the 33rd SLAC Summer Institute on Particle Physics (SSI 2005): Gravity in the Quantum World and the Cosmos. Menlo Park, USA: Stanford University eConf* (2005) .
- [10] LISA Pathfinder collaboration, *LISA Pathfinder: First steps to observing gravitational waves from space*, *Journal of Physics: Conference Series* **840** (2017) 012001.
- [11] M. Maggiore, C.V.D. Broeck, N. Bartolo, E. Belgacem, D. Bertacca, M.A. Bizouard et al., *Science case for the Einstein telescope*, *Journal of Cosmology and Astroparticle Physics* **2020** (2020) 050.

- [12] M. Punturo, M. Abernathy, F. Acernese, B. Allen, N. Andersson, K. Arun et al., *The Einstein Telescope: a third-generation gravitational wave observatory*, *Classical and Quantum Gravity* **27** (2010) 194002.
- [13] B.P. Abbott, R. Abbott, T.D. Abbott, F. Acernese, K. Ackley, C. Adams et al., *Multi-messenger observations of a binary neutron star merger*, *The Astrophysical Journal* **848** (2017) L12.
- [14] B.P. Abbott, R. Abbott, T.D. Abbott, S. Abraham, F. Acernese, K. Ackley et al., *Low-latency gravitational-wave alerts for multimessenger astronomy during the second advanced LIGO and virgo observing run*, *The Astrophysical Journal* **875** (2019) 161.
- [15] R. Abbott, T.D. Abbott, F. Acernese, K. Ackley, C. Adams, N. Adhikari et al., *Search for gravitational waves associated with gamma-ray bursts detected by Fermi and Swift during the LIGO–Virgo run O3b*, *The Astrophysical Journal* **928** (2022) 186.
- [16] LIGO SCIENTIFIC COLLABORATION AND VIRGO COLLABORATION collaboration, *Methods and results of a search for gravitational waves associated with gamma-ray bursts using the geo 600, ligo, and virgo detectors*, *Phys. Rev. D* **89** (2014) 122004.
- [17] E. Bissaldi, *Multi-messenger observations of GRBs: The GW connection*, *arXiv e-prints* (2019) arXiv:1909.05960.
- [18] S. Valenti, J.S. David, S. Yang, E. Cappellaro, L. Tartaglia, A. Corsi et al., *The discovery of the electromagnetic counterpart of GW170817: Kilonova AT 2017gfo/DTL17ck*, *The Astrophysical Journal* **848** (2017) L24.
- [19] Y.-F. Wang and A.H. Nitz, *Search for coincident gravitational wave and fast radio burst events from 4-OGC and the first CHIME/FRB Catalog*, *The Astrophysical Journal* (2022) .
- [20] R. Abbott, T.D. Abbott, S. Abraham, F. Acernese, K. Ackley, A. Adams et al., *Searches for continuous gravitational waves from young supernova remnants in the early third observing run of advanced LIGO and Virgo*, *The Astrophysical Journal* **921** (2021) 80.
- [21] J. Aasi, J. Abadie, B.P. Abbott, R. Abbott, T. Abbott, M.R. Abernathy et al., *Gravitational waves from known pulsars: Results from the initial detector era*, *The Astrophysical Journal* **785** (2014) 119.
- [22] V. Connaughton, E. Burns, A. Goldstein, L. Blackburn, M.S. Briggs, B.-B. Zhang et al., *Fermi GBM observations of LIGO gravitational-wave event GW150914*, *The Astrophysical Journal* **826** (2016) L6.
- [23] V. Connaughton, E. Burns, A. Goldstein, L. Blackburn, M.S. Briggs, N. Christensen et al., *On the interpretation of the Fermi-GBM transient observed in coincidence with LIGO gravitational-wave event GW150914*, *The Astrophysical Journal* **853** (2018) L9.
- [24] A. Goldstein, R. Hamburg, J. Wood, C.M. Hui, W.H. Cleveland, D. Kocevski et al., *Updates to the Fermi GBM targeted sub-threshold search in preparation for the third observing run of LIGO/Virgo*, *arXiv e-prints* (2019) arXiv:1903.12597.

- [25] D. Kocevski, E. Burns, A. Goldstein, T.D. Canton, M.S. Briggs, L. Blackburn et al., *Analysis of sub-threshold short gamma-ray bursts in Fermi GBM data*, *The Astrophysical Journal* **862** (2018) 152.
- [26] A. Loeb, *Electromagnetic counterparts to black hole mergers detected by ligo*, *The Astrophysical Journal* **819** (2016) L21.
- [27] L. Dai, J.C. McKinney and M.C. Miller, *Energetic constraints on electromagnetic signals from double black hole mergers*, *Monthly Notices of the Royal Astronomical Society: Letters* **470** (2017) L92.
- [28] J.M. Fedrow, C.D. Ott, U. Sperhake, J. Blackman, R. Haas, C. Reisswig et al., *Gravitational waves from binary black hole mergers inside stars*, *Phys. Rev. Lett.* **119** (2017) 171103.
- [29] R. Perna, D. Lazzati and B. Giacomazzo, *Short gamma-ray bursts from the merger of two black holes*, *The Astrophysical Journal* **821** (2016) L18.
- [30] S.E. Woosley, *The progenitor of GW150914*, *The Astrophysical Journal* **824** (2016) L10.
- [31] S.S. Kimura, S.Z. Takahashi and K. Toma, *Evolution of an accretion disc in binary black hole systems*, *Monthly Notices of the Royal Astronomical Society* **465** (2016) 4406.
- [32] B. Zhang, *Mergers of charged black holes: Gravitational-wave events, short gamma-ray bursts, and fast radio bursts*, *The Astrophysical Journal* **827** (2016) L31.
- [33] P. Veres, R.D. Preece, A. Goldstein, P. Mészáros, E. Burns and V. Connaughton, *Gravitational-wave observations may constrain gamma-ray burst models: The case of GW150914–GBM*, *The Astrophysical Journal* **827** (2016) L34.
- [34] P. Veres, T.D. Canton, E. Burns, A. Goldstein, T.B. Littenberg, N. Christensen et al., *Fermi-GBM follow-up of LIGO-Virgo binary black hole mergers: Detection prospects*, *The Astrophysical Journal* **882** (2019) 53.
- [35] S. De Mink and A. King, *Electromagnetic signals following stellar-mass black hole mergers*, *The Astrophysical Journal Letters* **839** (2017) L7.
- [36] A. Khan, V. Paschalidis, M. Ruiz and S.L. Shapiro, *Disks around merging binary black holes: From gw150914 to supermassive black holes*, *Phys. Rev. D* **97** (2018) 044036.
- [37] M. Maggiore, *Gravitational waves: Volume 1: Theory and experiments*, OUP Oxford (2007).
- [38] B. Paczynsky and P. Wiita, *Thick accretion disks and supercritical luminosities.*, *Astronomy and Astrophysics* **500** (1980) 203.
- [39] M.A. Abramowicz, *The Paczyński-wiita potential. A step-by-step "derivation" - commentary on: Paczyński b. and wiita p. j., 1980, astronomy & astrophysics, 88, 23*, *Astronomy & Astrophysics* **500** (2009) 213.

- [40] U. Torkelsson, *The special and general relativistic effects on orbits around point masses*, *European journal of physics* **19** (1998) 459.
- [41] V. Witzany, O. Semerák and P. Suková, *Free motion around black holes with discs or rings: between integrability and chaos IV*, *Monthly Notices of the Royal Astronomical Society* **451** (2015) 1770.
- [42] P.J. Prince and J.R. Dormand, *High order embedded runge-kutta formulae*, *Journal of computational and applied mathematics* **7** (1981) 67.
- [43] A.H. Barnett, J.F. Magland and L.a. Klinteberg, *A parallel non-uniform fast fourier transform library based on an "exponential of semicircle" kernel*, *SIAM Journal on Scientific Computing* **41** (2019) C479.
- [44] A.H. Barnett, *Aliasing error of the $\exp(\beta\sqrt{1-z^2})$ kernel in the nonuniform fast fourier transform*, *arXiv e-prints* (2020) arXiv:2001.09405.
- [45] M.P. van Haarlem, M.W. Wise, A.W. Gunst, G. Heald, J.P. McKean, J.W.T. Hessels et al., *Lofar: The low-frequency array*, *Astronomy and Astrophysics* **556** (2013) A2.
- [46] M.P. van Haarlem, M.W. Wise, A.W. Gunst, G. Heald, J.P. McKean, J.W.T. Hessels et al., *LOFAR: The LOw-frequency ARray*, *Astronomy & Astrophysics* **556** (2013) A2.